

**Discovery of a potent and highly fluorescent sirtuin inhibitor**

Journal:	<i>MedChemComm</i>
Manuscript ID:	MD-CAR-07-2015-000307.R1
Article Type:	Concise Article
Date Submitted by the Author:	23-Aug-2015
Complete List of Authors:	Yeong, Keng Yoon; Universiti Sains Malaysia, Institute for Research in Molecular Medicine Mohamed, Ashraf Ali; Institute for Research in Molecular Medicine (INFORM) , Pharmacogenetic and Novel Therapeutics; Alwar Pharmacy College, Drug Discovery Research ANG, CHEE WEI; UNIVERSITI SAINS MALAYSIA, Tan, Soo Choon; Universiti Sains Malaysia, Institute for Research in Molecular Medicine Nasrolahi Shirazi, Amir; University of Rhode Island, Biomedical and Pharmaceutical Sciences Parang, Keykavous; University of Rhode Island,



Journal Name

COMMUNICATION

Discovery of a potent and highly fluorescent sirtuin inhibitor

Y. K. Yoon^{a*}, M. A. Ali^a, A. C. Wei^a, T. S. Choon^a, A. N. Shirazi^b, K. Parang^b

Received 00th January 20xx,
Accepted 00th January 20xx

DOI: 10.1039/x0xx00000x

www.rsc.org/

In search for potent sirtuins inhibitors, a series of diversified 1,2-disubstituted benzimidazole analogues were synthesized using a one-pot method. The most potent compound in the series (BZD9L1), was discovered to show high autofluorescence which can be utilized to predict its localization in cells. More importantly, BZD9L1 displayed high antiproliferative effects against a panel of cancer cells tested. Molecular docking studies also help to explain the observed structure-activity-relationship.

Introduction

Fluorescent imaging using fluorescently tagged drug molecules is a popular tool used in the area of biomedical sciences to gain insight into cellular mechanism.¹⁻³ This was extremely interesting as pharmacological phenomena involving the ligand and receptor which was hypothetical, could be visualized.

However, the early excitement fizzled out as researchers remained skeptical regarding the pharmacological properties of compounds that have been changed by the addition of the fluorescent tags.⁴ Alternatively, sophisticated labeling techniques such as multi-step staining method would not allow live imaging concurrent with drug treatment. Therefore, an autofluorescent drug is beneficial as it can show the interaction between drug and receptor minus the disadvantages mentioned above. Nevertheless, emergence of new autofluorescence drugs is relatively limited.⁵⁻⁷

Inhibition of sirtuins has been promoted as among the newest

strategies in combating cancer. Advances in sirtuin biology has been increasing at a fast pace for the past decade. Sirtuins (SIRT1-7) are NAD⁺-dependent class III HDACs that share extensive homologies with the yeast HDAC Sir2.⁸ Several Class I and class II HDACs inhibitors have been approved for cancer treatment (Vorinostat, romidepsin, belinostat, panobinostat)⁹⁻¹⁰ but much less is known about class III HDAC inhibitors. Lately, sirtuins activities have been linked to cancer^{11,12} as well as neurological diseases such as Parkinson's¹³ and Alzheimer.¹⁴ Both SIRT1 and SIRT2 are also believed to have a role in the development of cancer as their functions are frequently altered in cancer cells.¹⁵⁻¹⁸

Further refinement of the active scaffold from our previous work^{19,20} by molecular modeling postulated a better fit of the compounds into the enzyme cavities without bulky substitution at position-1 (data not shown) of the benzimidazole moiety. Herein we would like to report novel highly fluorescent sirtuin inhibitors which contained the benzimidazole core structure. Molecular docking experiments provided insight into the binding mode of these novel benzimidazoles while their fluorescence properties gave clues to their localization in cell.

Experimental

Chemistry

All chemicals were supplied by Sigma-Aldrich (U.S.A) and Merck Chemicals (Germany). Thin layer chromatography (TLC) using silica gel G was performed in the solvent system chloroform-methanol (9:1). The spots were located under short (254nm)/long (365nm) UV light. Elemental analyses were measured on Perkin Elmer 2400 Series II CHN Elemental Analyzer and were within $\pm 0.4\%$ of the calculated values. ¹H and ¹³C NMR were performed on Bruker Avance 300/500 (¹H: 300/500 MHz, ¹³C: 75/125 MHz) spectrometer in CDCl₃ using TMS as internal standard. Mass spectra were recorded on Varian 320-MS TQ LC/MS in positive ESI mode. Absorption spectra were recorded on Agilent 8453 UV-visible spectrophotometer. Fluorescence emission spectra were recorded

^a Institute for Research in Molecular Medicine, Universiti Sains Malaysia, Minden, 11800, Penang, Malaysia.

^b Department of Biomedical and Pharmaceutical Sciences, College of Pharmacy, University of Rhode Island, Kingston, RI, 02881, United States.

† Electronic Supplementary Information (ESI) available: Compound characterization data, Supplementary biological data, additional photochemical measurements and molecular docking analyses. See DOI: 10.1039/x0xx00000x

on Agilent Cary Eclipse Fluorescence spectrophotometer. Immunoblots were captured with Bio-Rad Chemidoc XRS System Imager. Fluorescence images were captured using AMG EVOS fluorescent digital inverted microscope. Melting point was performed on Gallenkamp MFB595.010M Melting Point apparatus.

General procedure for the synthesis of ethyl-(2-substituted)-benzo[d]imidazole-5-carboxylate:

4-fluoro-3-nitrobenzoic acid (0.05 g, 0.27 mmol) was esterified in the presence of catalytic H₂SO₄ in EtOH (10 mL) by refluxing at 65 °C for 6 h (TLC). Various amines (0.26 mmol) were subsequently added to the solution, stirred for 0.5 h, treated with SnCl₂ (190 mg, 1 mmol) and stirred for a further 0.5 h. The resulting mixture was then treated with various aldehydes (0.3 mmol) and NaHSO₃ (57 mg, 0.3 mmol) and left to stir for another 3 h. The solution was cooled to room temperature and subsequently evaporated under reduced pressure. It was resuspended in EtOAc (10 mL), washed with 10% Na₂CO₃ (20 mL) and water (20 mL x 2), dried over Na₂SO₄ and concentrated under reduced pressure. The crude products were purified by column chromatography (silica gel, 70-230 mesh; CHCl₃-MeOH 9:1) to obtain the final products (73-92%).

Physicochemical Properties

Aqueous solubility analysis and molar extinction coefficient

Aqueous solubility (with 0.5% DMSO) of BZD9L1 was determined using a UV spectrophotometric method. A series of dilution was made from BZD9L1 dissolved in DMSO. These solutions were analyzed by UV spectroscopy and their absorbance at 346 nm was plotted against concentration. The molar extinction coefficient was calculated from the gradient of the line of best fit.

The aqueous solubility of BZD9L1 was determined by diluting 10.5 µL of a 40 mM DMSO solution to 1 mL with water. An aliquot of this solution (60 µL) was added to water (40 µL) and any undissolved compound was pelleted by centrifugation. The supernatant (80 µL) was diluted to 4 mL with DMSO and subsequently analyzed by UV spectroscopy.

Quantum yield

The fluorescence emission spectra of BZD9L1 dissolved in DMSO were taken in a quartz cuvette (10 mm × 10 mm), using Agilent Cary Eclipse fluorescence spectrophotometer with emission slit width of 5 nm. The excitation wavelength was set at 346 nm.

The quantum yield (Φ) was calculated by preparing solutions of the sample at varying concentrations in DMSO, and measuring the absorbance at 346 nm and the fluorescence emission peak at each different concentration. The absorbance peak was plotted against emission peak and compared to a standard of known quantum yield (quinine sulphate). This data was used to obtain a value for the quantum yield.

The quantum yield of BZD9L1 in DMSO was calculated using the following equation:

$$\Phi = \Phi_R(\text{Grad/Grad}_R)(\eta^2/\eta_R^2)$$

Φ = Quantum yield

Φ_R = Quantum yield of reference

η = refractive index of sample

η_R = refractive index of reference

Quinine Sulphate was used as reference, which has a quantum yield of 54.6% when dissolved in 0.5 M H₂SO₄. Refractive index of 0.5M H₂SO₄ is 1.346, while refractive index of DMSO is 1.479 and refractive index of 0.01M PBS is 1.334.

Biological

Enzymatic Assay

SIRT1 *in vitro* assay

3.3 µM of SIRT1 substrate derived from human p53 sequences, 66.7 µM NAD⁺, 50 µM of interested compounds (all final concentration) and 0.5 µg of SIRT1 human recombinant (GenBank Accession #: NM_012238) with 193- 741 amino acids and GST tag at its N-terminal, were incubated for 45 minutes at 37°C. 50 µL of stop solution consisting nicotinamide and SIRT1 developer was then added and the mixture was incubated for a further 10 minutes at 37°C. Fluorescence was measured at 490 nm (excitation) and 520 nm (emission) and the inhibition was calculated as the ratio of absorbance under each experimental condition to that of the control.

SIRT2 *in vitro* assay

6.7 µM of SIRT2 substrate derived from human p53 sequences, 333 µM NAD⁺, 50 µM of interested compounds (all final concentration) and 0.5 µg of SIRT2 human recombinant (GenBank Accession #: NM_030593) with 13- 319 amino acids and His tag at its C-terminal, were incubated for 45 minutes at 37°C. 50 µL of stop solution consisting nicotinamide and SIRT1 developer was then added and the mixture was incubated for a further 10 minutes at 37°C. Fluorescence was measured at 490 nm (excitation) and 520 nm (emission) and the inhibition was calculated as the ratio of absorbance under each experimental condition to that of the control.

Western Blot

HCT116 cell line was obtained from the American Type Culture Collection. HCT116 cells were maintained in RPMI media (Biowest, USA) containing 10% FCS and 1% Penicillin-Streptomycin. All final concentrations of solvent were identical between and within experiments; SIRT inhibitors - EX-527 (Tocris Bioscience, UK), AGK2 (Tocris Bioscience) and BZD9L1 were dissolved in stock solutions of 50 mM in DMSO. For treatments, the compounds were diluted in DMSO to the appropriate concentrations and added to cells (0.5% v/v final DMSO concentration).

HCT116 cells were seeded at a density of 4 × 10⁵ in 6-well plates. Cells were treated with various SIRT inhibitors for 24 h and subsequently lysed in 8M urea buffer containing protease inhibitor cocktail (Nacalai Tesque, Japan). Total cell lysates were denatured and resolved on SDS-polyacrylamide gels and transferred onto PVDF membranes (Amersham, UK).

Western blots were performed using the following antibodies: monoclonal acetylated α -tubulin (1:1000; CST, USA), monoclonal acetylated p53 (1:1000; Abcam, UK), monoclonal β -actin (1:5000; Sigma-Aldrich, USA). Primary antibodies were detected using horseradish peroxidase linked to anti-mouse and anti-rabbit conjugates as appropriate (1:3000; CST, USA) and visualized using the enhanced chemiluminescence detection reagent (Amersham, UK).

Cell Proliferation Assay

All cell lines were obtained from the American Type Culture Collection (Rockville, MD). Cells were seeded in 96-well plates at a density of 5×10^3 per well. The cells were treated with 50 μ M of interested compounds and allowed to adhere for 72 hours. Then, the proliferative activity was determined by 3-(4,5-dimethylthiazol-2-yl)-5-(3-carboxymethoxyphenyl)-2-(4-sulfophenyl)-2H-tetrazolium, inner salt assay (CellTiter 96 AQueous Non-Radioactive Cell Proliferation Assay; Promega, Madison, WI) to monitor the number of viable cells according to the manufacturer's instructions. Briefly, 3-(4,5-dimethylthiazol-2-yl)-5-(3-carboxymethoxyphenyl)-2-(4-sulfophenyl)-2H-tetrazolium, inner salt solution was added at 20 μ L/well, and after 1 hour of incubation at 37°C in a humidified 5% CO₂ atmosphere, the conversion of 3-(4,5-dimethylthiazol-2-yl)-5-(3-carboxymethoxyphenyl)-2-(4-sulfophenyl)-2H-tetrazolium, inner salt to formazan was measured in a plate reader at 490 nm. All experiments were done in triplicate, and the proliferation rate was calculated as the ratio of absorbance under each experimental condition to that of the control.

Molecular docking

The crystal structure of human SIRT2 (PDB code: 3ZGV) was taken from the Protein Data Bank. Monomer A was selected from the dimeric SIRT2 structure of 3ZGV as SIRT2 is a monomer in solution. The receptor and ligands were structurally optimized prior to the actual docking simulation. After removing the co-crystallized water molecules, hydrogen atoms were added to the protein structure. Ligands were energy minimized with Chem 3D Pro 13.0 using the MM2 forcefield.

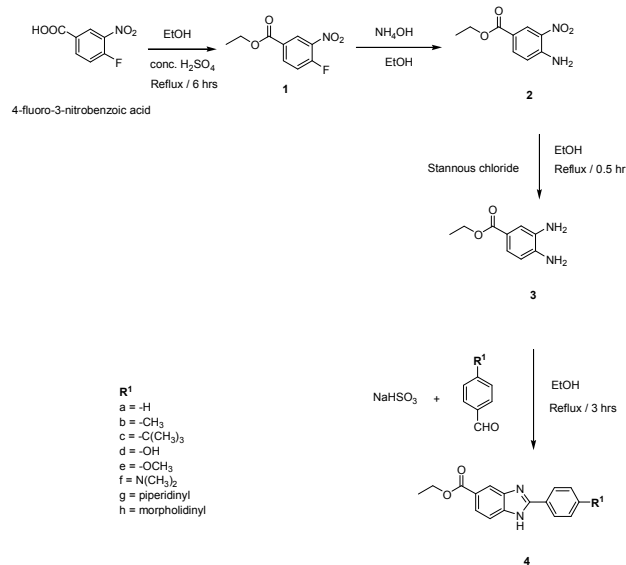
Docking of the co-crystallized ADPr as well as other interested ligands (BZD9L1, 4d and 4e) were carried out using Autodock 4.2. Control dock of ADPr against 3ZGV was performed and it gave a low rmsd value (0.891 Å), implying a reliable docking protocol was used. For each molecule, 10 docking runs were performed. The top-ranked pose for each ligand were retained and further analyzed with Maestro 9.8 or VMD 1.9.1 molecular graphics software.

Results and discussion

Synthesis of compounds

The synthetic scheme is a four-step pathway (Scheme 1) leading to the formation of a variety of benzimidazole derivatives as described previously.²¹

The starting material, 4-fluoro-3-nitro benzoic acid was esterified in the presence of catalytic sulfuric acid in ethanol by refluxing for 6 hours to afford 1. Ammonium hydroxide was subsequently added into the solution and subsequently stirred at room temperature for 0.5 hour. The resultant intermediate, 2 was then reduced to 3 using stannous chloride. The phenylenediamine 3 was then mixed with various substituted benzaldehyde to afford benzimidazole derivatives 4a-h in good yields (73-92%).



Scheme 1. Synthesis protocol of benzimidazole derivatives 4a-h

Enzymatic Assays

The *in vitro* enzymatic screening assay for SIRT1 and SIRT2 inhibitory activity were performed using fluorimetric drug discovery kits (AnaSpec, Fremont, CA) according to the manufacturer's protocol. EX-527 (selective for SIRT1), AGK2 (selective for SIRT2), and Tenovin-6 (pan-SIRT1/2 inhibitors), were used as standard control while DMSO was used as a vehicle control. Experiments were performed in triplicates and standard deviations obtained from all experiments are less than 20%.

Our previous results showed that strong electron donating substitution at R¹ position gave potent sirtuin inhibitory activity. Therefore, we synthesized compounds with substitution from weak to strong electron donating groups at R¹ position probe in greater detail. It was noted that strong electron donating substitution with basic side chain such as dimethylamino and piperidinyl groups give the best inhibitory activity (Table 1).

Intriguingly, the importance of the side chain basicity was also observed with naphthalimide for their cytotoxicity activity as reported by Braña et al.²² Further confirmation of this effect was confirmed when weakened inhibitory effect was observed with morpholinyl group replacing piperidinyl group at the R¹ position.

Strong electron donating groups were postulated to help in stabilizing the benzimidazole core and this in turn gave stronger interaction between the imidazole moiety and important amino acids in the active site of the enzyme (discussed in molecular docking section).

Table 1. SIRT1 and SIRT2 inhibitory activities of benzimidazole derivatives 4a-h

Compound	SIRT1 inhibition (%) at 50 μM	IC ₅₀ SIRT1 inhibition (μM)	SIRT2 inhibition (%) at 50 μM	IC ₅₀ SIRT2 inhibition (μM)
4a	24.70	N.D.	36.31	N.D.
4b	40.11	N.D.	45.16	N.D.
4c	46.92	N.D.	50.20	N.D.
4d	37.36	N.D.	42.93	N.D.
4e	19.70	N.D.	26.01	N.D.
4f	43.93	62.9 \pm 8.8	87.55	13.6 \pm 2.5
4g (BZD9L1)	55.08	42.9 \pm 5.3	93.20	9.0 \pm 1.4
4h	37.77	57.5 \pm 10.3	60.74	52.91 \pm 4.6
Ex-527	N.D.	0.25 \pm 0.05	N.D.	43.7 \pm 2.0
AGK2	N.D.	68 \pm 9.4	N.D.	7.9 \pm 1.5
Tenovin-6	N.D.	47.8 \pm 2.9	N.D.	27.0 \pm 2.1

N.D. = Not determined

The inhibition potency was however, greatly affected when the substitution was replaced by other electron donating groups such as methyl ($-\text{CH}_3$), *tert*-butyl ($-\text{C}(\text{CH}_3)_3$). However, what was surprising was that even strong electron donating groups such as methoxy ($-\text{OCH}_3$) and hydroxyl ($-\text{OH}$) gave poor inhibition. This phenomenon was probed in more detail through molecular docking studies (see molecular docking section). Compound **4g** (codenamed **BZD9L1**, Figure 1) was demonstrated to be the most potent inhibitor of the series (SIRT1 IC₅₀ = 42.9 μM ; SIRT2 IC₅₀ = 9.0 μM). It was found to be a pan-SIRT1/SIRT2 inhibitor; albeit with a preference to inhibit SIRT2 over SIRT1.

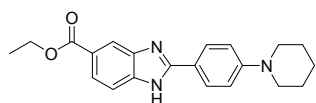


Figure 1. Structure of **BZD9L1**

To examine the mechanism of sirtuin inhibition by **BZD9L1**, we first determined whether inhibition by **BZD9L1** was time-dependent. The time course of product formation was monitored in the absence and presence of **BZD9L1**. From the experiment, **BZD9L1** was found to exhibit linear progress curves over time. These data suggest that **BZD9L1** is a reversible inhibitor for both SIRT1 and SIRT2 (supporting information).

As **BZD9L1** was found to have greater affinity towards SIRT2, further analysis of **BZD9L1** was targeted towards SIRT2. The binding mode of **BZD9L1** towards SIRT2 was analyzed using competition analysis following method adopted from Lai et al.²³ The inhibition of **BZD9L1** was tested with increasing concentration of NAD^+ while the other parameters of the assay were kept constant. Competition analysis demonstrated that **BZD9L1** is competitive with respect to NAD^+ which implies that the inhibitor competes with NAD^+ to occupy the same binding site in the receptor (Figure 2).

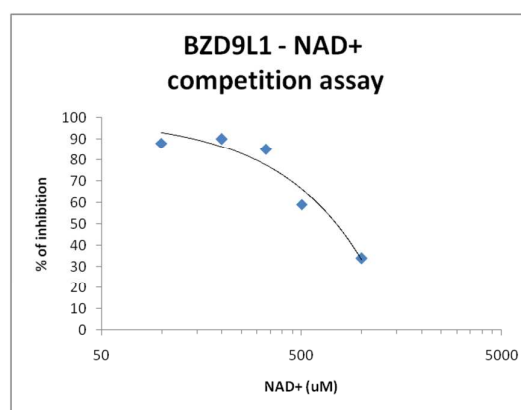
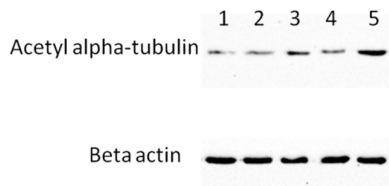


Figure 2. Decreasing SIRT2 inhibition by **BZD9L1** with increasing concentrations of NAD^+

In light of the reported issues surrounding certain *in vitro* SIRT assays,²⁴ it was crucial to validate the *in vitro* results in cells. Before carrying out the cell-based assay, aqueous solubility of **BZD9L1** was determined following a spectroscopic method modified from McCarthy et al.²⁵ Determination of aqueous solubility at this point was deemed critical as it not only give the benchmark of the concentration to use in cell-based studies but it also serve as a guide whether it is worth to further investigate the compound as poor water solubility might limit its use *in vivo*. The solubility of **BZD9L1** in water (with 0.5% DMSO) was determined to be 20.8 $\mu\text{g}/\text{mL}$ (59 μM) and additional functional tests were then conducted on **BZD9L1** (up to 50 μM final concentration) to ascertain its ability to inhibit sirtuin enzymes in a cellular context. Thus, acetylation status of p53 and α -tubulin, which are well established direct cellular biomarkers of SIRT1 and SIRT2 respectively, was monitored in HCT116 cancer cells (Figure 3). Hyperacetylation of α -tubulin was duly observed while for p53 the signal was barely noticeable. This could be due to the fact that p53 is normally expressed at very low levels in wild type p53 cells without DNA damage. It was previously shown that SIRT1 inhibition could be quantified in cells by

determining the level of p53 acetylation following induction of DNA damage by the genotoxic agent etoposide.²⁶

A



B

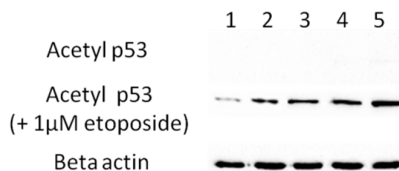


Figure 3. Effects of sirtuin inhibitors on alpha-tubulin (A) and p53 (B) acetylation. Control (1); 10 μ M EX-527 (2); 10 μ M AGK2 (3); 10 μ M **BZD9L1** (4); 50 μ M **BZD9L1** (5).

We next treated the HCT-116 cells with **BZD9L1** in the presence of 1 μ M etoposide. As expected, **BZD9L1** showed significantly higher level of p53 acetylation in a dose-response manner. However, it has to be pointed out that p53 can also in part be deacetylated by SIRT2. Beta-actin was used as loading control.

Molecular docking

In an attempt to rationalize the observed *in vitro* enzymatic activities, docking study of the benzimidazole derivatives into the active site of human SIRT2 was performed (PDB entry code: 3ZGV, x-ray resolution = 2.30 Å).²⁷ The receptor and the drug candidates were optimized before actual docking in Autodock 4.2 using standard procedure of the software.

BZD9L1 was found to overlap nicely with adenosine diphosphate ribose (ADPr) in the active site of SIRT2 (Figure 4).

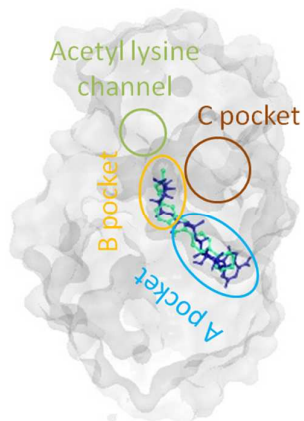


Figure 4. **BZD9L1** docked into the active site of SIRT2. **BZD9L1** (green) docked into the active site of SIRT2. It was postulated to compete with NAD^+ as it was found to overlap nicely with ADPr (blue), occupying the "A" and "B" pockets.

This is in agreement with our NAD^+ competition assay result. In the case of compound 4d (-OH) and 4e (-OCH₃) which contained strong electron donating substituent at R¹ position, the docking analysis showed that they are shifted out from the ADPr binding site with different binding orientation, resulting in less favorable complexes (supporting information).

The docking analysis reveals that the **BZD9L1** interacts with receptor primarily due to hydrogen bonding as well as anion lone pair- π interactions. Accommodation of **BZD9L1** into the ADPr binding site of SIRT2 was favoured by a hydrogen bond with the backbone of Gln167 and N from imidazole of **BZD9L1** (Figure 5).

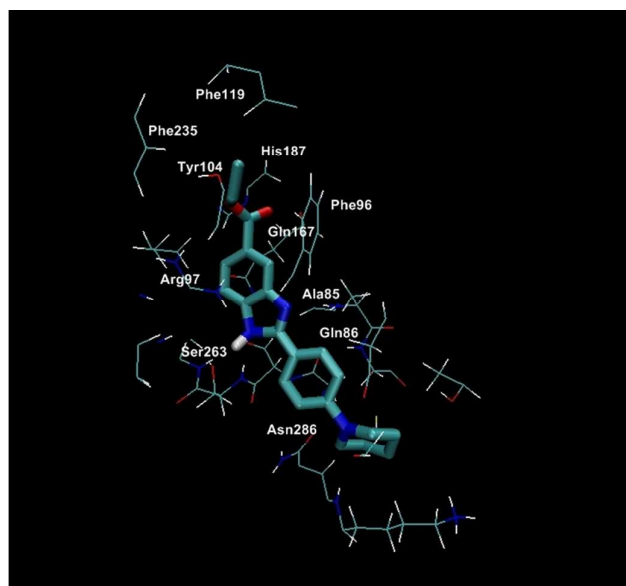


Figure 5. Molecular interactions between **BZD9L1** and SIRT2. Molecular interactions observed between **BZD9L1** and SIRT2 (within 5Å). Important interactions include those with Gln167, Gly86, Arg97, His187 and Phe96. (PDB code: 3ZGV)

Hydrogen bond was also observed between Gly86 and imidazole ring of **BZD9L1** as well as between Arg97 and ester chain of **BZD9L1**. Lone pair- π interactions with His187 as well as Phe96 also help to stabilize the complex. Alterations to these amino acids are deemed crucial to the inhibition of SIRT2 enzyme.^{28,29} In general, the interactions observed between SIRT2 and **BZD9L1** are relatively consistent with the hydrogen bonds observed between reported SIRT2 and ADPr complex.²⁷ Other prominent interactions include those with Ser263, Thr262 and Ala85. Certain hydrophobic van der Waals interaction were also noted with Tyr104, Phe235 and Phe119 which are located at the gauge opening of the acetyl lysine channel.

Fluorescence Properties

We discovered that the most potent compound, BZD9L1, possessed intrinsic fluorescence when light-irradiated at $\lambda_{\text{ex}} = 346$ nm with emission maximum at $\lambda_{\text{em}} = 448$ nm. It was found to be highly fluorescent with a measured molar extinction coefficient, ϵ , of 23000 ($\pm 15\%$). Its quantum yield was found to be 33.7% ($\pm 15\%$) in DMSO, with quinine sulfate dihydrate in 0.5 M H_2SO_4 as the reference (supporting information). In buffer (0.5% DMSO/0.01M PBS), the molar extinction coefficient, ϵ , was 19000 while its quantum yield dropped to 1.5%.

Although the fluorescence intensity of BZD9L1 was significantly reduced in buffer, the intensity was still strong enough for it to be used to study the localization of BZD9L1 in cells. The cellular distribution of BZD9L1 was studied by fluorescence microscopy in living HCT116 colon cancer cells as well as CCD18 colon fibroblast. Bright-field images of both HCT116 and CCD18 cells treated with BZD9L1 (50 μM in 0.5% DMSO/0.01M PBS) were taken prior to fluorescence microscopy imaging to ensure that the cells were morphologically intact (Figure 6A, B).

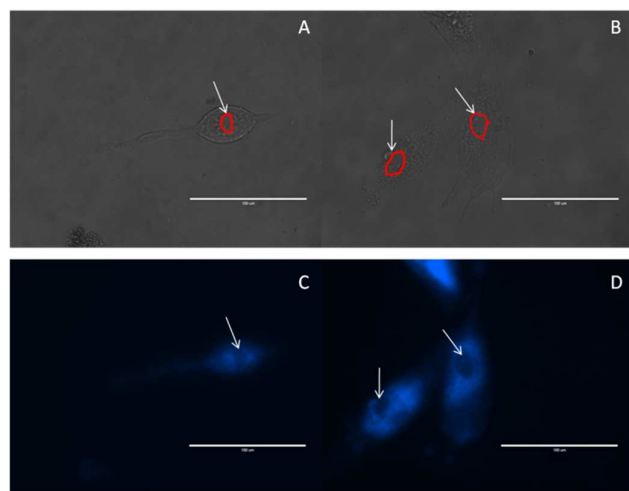


Figure 6. Fluorescence microscopy images of BZD9L1 in cells. Live-cell images of HCT116 colon cancer cell (A, C) and CCD18 colon fibroblast (B, D) incubated with BZD9L1. (A, B) Bright-field images; (C, D) fluorescence images. Arrows point to cell nucleus. Bar represents 100 μm .

Fluorescence images showed that BZD9L1 were taken up by both types of cell and diffused quickly inside the cells. Cellular distribution can be visualized within minutes of incubation. It was shown that BZD9L1 have high affinity towards the cytoplasm of both cell types (Figure 6C, D). This is consistent with our *in vitro* enzymatic assay finding where BZD9L1 showed inhibition against SIRT2, which is localized in the cytoplasm. Although predominantly located in the nucleus, SIRT1 was shown to shuttle to cytoplasm in certain cancer cells.³⁰ Therefore, localization of BZD9L1 in the cytoplasm does not rule out the inhibition of SIRT1 in cancer cells.

Cell proliferation Assays

The antitumor activity of various known sirtuin inhibitors has been previously demonstrated in the literature.³¹ Thus, the growth

inhibitory activities of the synthesized compounds were evaluated on a panel of human cancer cells by the MTS assay after 72 h of incubation at 50 μM concentration. As shown in Figure 7, preliminary studies showed that BZD9L1 gave the best cytotoxic activity against all three cancer cells tested (HCT116, CCRF-CEM and MDA-MB-468), followed by 4f, while less pronounced effect was observed for the other compounds with inferior SIRT2 inhibition. Interestingly, this resembled the trend obtained from the *in vitro* SIRT2 enzymatic inhibitory results, implying the correlation between sirtuin inhibition and antiproliferation of cancer cells. The results also demonstrate the broad spectrum ability of BZD9L1 in inhibiting cancer cell growth. Standard deviation obtained for all experiments are less than 15% (supporting information).

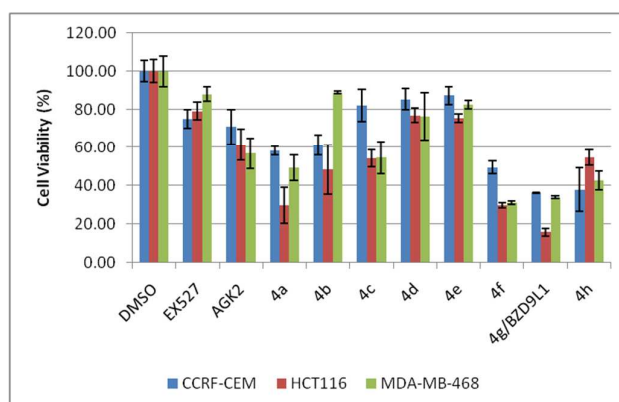


Figure 7. Antiproliferative activity of synthesized compounds 4a-h against HCT-116, MDA-MB-468 and CCRF-CEM cells.

Conclusions

In conclusion, we have discovered a potent sirtuin inhibitor (BZD9L1) which is the first highly fluorescent sirtuin inhibitor described so far. Results demonstrated that BZD9L1 can be visualized with fluorescence microscopy in living cells without any conjugation to external fluorophores. Uptake of the compound in cells is fast and it is localized predominantly in cell cytoplasm. The intrinsic fluorescence properties of BZD9L1, a feature fairly uncommon among anticancer drugs, may prove useful in monitoring morphological as well as phenotype changes in cancer cells.

Furthermore, BZD9L1 displayed high antiproliferative effects across a panel of cancer cell lines (HCT116, CCRF-CEM and MDA-MB-468), thus suggesting this compound as a promising candidate for cancer treatment. This scaffold warrant continuous exploration as it may yield useful compounds that could be used to interrogate the biology of sirtuins. Further work in this area is currently on-going in our laboratory.

Acknowledgements

The authors wish to express their gratitude to Pharmacogenetics and Novel Therapeutics Research Cluster, Institute for Research in Molecular Medicine, Universiti Sains Malaysia, Penang for supporting this work. The authors also will like to thank Dr C.E. Oon for her comments in cell-based assays and Dr. M.L. Tan for the use of immunoblot imager. This work was funded through Research Grant No. RUC (1001/PSK/8620012) and FRGS Grant No. (203/C1PPM/6711335).

Notes and references

- McGrath, J. C.; Arribas, S. M.; Daly, C. J. *Trends Pharmacol. Sci.*, **1996**, *17*, 393–399.
- Baker, J. G.; Hall, I. P.; Hill, S. J. *Br. J. Pharmacol.*, **2003**, *139*, 232–242.
- Ntziachristos, V. *Annu. Rev. Biomed. Eng.*, **2006**, *8*, 1–33.
- McGrath, J. C.; Daly, C. J. *Br. J. Pharmacol.*, **2003**, *139*, 187–189.
- Burke, T. G.; Malak, H.; Gryczynski, I.; Mi, Z.; Lakowicz, J. R. *Anal. Biochem.*, **1996**, *242*, 266–270.
- Renault, E.; Fontaine-Aupart, M. P.; Tfibel, F.; Gardes-Albert, M.; Bisagni, E. *J. Photochem. Photobiol. B: Biol.*, **1997**, *40*, 218–227.
- Husain, N.; Agbaria, R. A.; Warner, I. M. *J. Phys. Chem.*, **1993**, *97*, 10857–10861.
- Blander, G.; Guarente, L. *Annu. Rev. Biochem.* **2004**, *73*, 417–435
- Mottamal, M.; Zheng, S.; Huang, T.L.; Wang, G. *Molecules*, **2015**, *20*, 3898–3941.
- FDA approves Farydak for treatment of multiple myeloma. Available online: <http://www.fda.gov/NewsEvents/Newsroom/PressAnnouncements/ucm435296.htm>
- Saunders, L. R.; Verdin, E. *Oncogene*, **2007**, *26*, 5489–5504
- Bosch-Presegue, L.; Vaquero, A. *Genes Cancer*, **2011**, *2*, 648–662
- Chen, J.; Zhou, Y.; Mueller-Steiner, S.; Chen, L. F.; Kwon, H.; Yi, S.; Mucke, L.; Gan, L. *J. Biol. Chem.*, **2005**, *280*, 40364–40374
- Garske, A. L.; Smith, B. C.; Denu, J. M. *ACS Chem. Biol.*, **2007**, *2*, 529–532
- Wang, R. H.; Sengupta, K.; Li, C.; Kim, H. S.; Cao, L.; Xiao, C.; Kim, S.; Xu, X.; Zheng, Y.; Chilton, B.; Jia, R.; Zheng, Z. M.; Appella, E.; Wang, X. W.; Ried, T.; Deng, C. X. *Cancer Cell*, **2008**, *14*, 312–323
- Deng, C. X. *Int. J. Biol. Sci.*, **2009**, *5*, 147–152
- Bradbury, C. A.; Khanim, F. L.; Hayden, R.; Bunce, C. M.; White, D. A.; Drayson, M. T.; Craddock, C.; Turner, B. M. *Leukemia*, **2005**, *19*, 1751–1759
- Huffman, D. M.; Grizzle, W. E.; Bamman, M. M.; Kim, J. S.; Eltoun, I. A.; Elgavish, A.; Nagy, T. R. *Cancer Res.*, **2007**, *67*, 6612–6618
- Yoon, Y. K.; Ali, M. A.; Wei, A. C.; Choon, T. S.; Osman, H.; Parang, K.; Shirazi, A. N. *Bioorg. Med. Chem.*, **2014**, *22*, 703–710.
- Yoon, Y. K.; Ali, M. A.; Wei, A. C.; Shirazi, A. N.; Parang, K.; Choon, T.S. *Eur. J. Med. Chem.*, **2014**, *83*, 448–454.
- Yoon, Y. K.; Ali, M. A.; Wei, A. C.; Choon, T. S.; Osman, H. *Tetrahedron Lett.*, **2014**, *55*, 4697–4700.
- Braña, M. F.; Cacho, M.; Gradillas, A.; de Pascual-Teresa, B.; Ramos, A. *Curr. Pharm. Des.*, **2001**, *7*, 1745–1780.
- Lai, C. J.; Wu, J. C. *Assay Drug Dev. Technol.*, **2003**, *1*, 527–535.
- Smith, B. C.; Hallows, W. C.; Denu, J. M. *Anal. Biochem.*, **2009**, *394*, 101–109.
- McCarthy, A. R.; Pirrie, L.; Hollick, J. J.; Sebastien, R.; Campbell, J.; Higgins, M.; Staples, O. D.; Tran, F.; Slawin, A. M. Z.; Lain, S.; Westwood, N. J. *Bioorg. Med. Chem.*, **2012**, *20*, 1779–1793
- Heltweg, B.; Gatbonton, T.; Schuler, A. D.; Posakony, J.; Li, H.; Goehle, S.; Kollipara, R.; Depinho, R. A.; Gu, Y.; Simon, J. A.; Bedalov, A. *Cancer Res.*, **2006**, *66*, 4368–4377.
- Moniot, S.; Schutkowski, M.; Steegborn, C. *J. Struct. Biol.*, **2013**, *182*, 136–143
- Finnin, M. S.; Donigian, J. R.; Pavletich, N. P. *Nat. Struct. Mol. Biol.*, **2001**, *8*, 621–625.
- Sakkiah, S.; Arooj, M.; Cao, G. P.; Lee, K. W. *PLoS One*, **2013**, *8*, e59278.
- Byles V., Chmielewski L.K., Wang J., Zhu L., Forman L.W., Faller D.V., Dai Y. *Int. J. Biol. Sci.*, **2010**, *6*, 599–612.
- Lara, E.; Mai, A.; Calvanese, V.; Altucci, L.; Lopez-Nieva, P.; Martinez-Chantar, M.L.; Varela-Rey, M.; Rotili, D.; Nebbioso, A.; Roperio, S.; Montoya, G.; Oyarzabal, J.; Velasco, S.; Serrano, M.; Witt, M.; Villar-Garea, A.; Inhof, A.; Mato, J.M.; Esteller, M.; Fraga, M.F. *Oncogene*, **2009**, *28*, 781–791.

GRAPHICAL ABSTRACT

